Journal of Biomedical Optics

SPIEDigitalLibrary.org/jbo

Ratio images and ultraviolet C excitation in autofluorescence imaging of neoplasms of the human colon

Timothy E. Renkoski
Bhaskar Banerjee
Logan R. Graves
Nathaniel S. Rial
Sirandon A. H. Reid
Vassiliki Liana Tsikitis
Valentine N. Nfonsam
Piyush Tiwari
Hemanth Gavini
Urs Utzinger

Ratio images and ultraviolet C excitation in autofluorescence imaging of neoplasms of the human colon

Timothy E. Renkoski,[a] Bhaskar Banerjee,[a,b,c] Logan R. Graves,[a] Nathaniel S. Rial,[b] Sirandon A. H. Reid,[b] Vassiliki Liana Tsikitis,[d] Valentine N. Nfonsam,[d] Piyush Tiwari,[b] Hemanth Gavini,[b] and Urs Utzinger[a,c]
[a]University of Arizona, College of Optical Sciences, 1630 E. University Boulevard, Tucson, Arizona 85721
[b]University of Arizona, Department of Medicine, Section of Gastroenterology, 1501 N. Campbell Avenue, P.O. Box 245028, Tucson, Arizona 85724-5028
[c]University of Arizona, Department of Biomedical Engineering, 1127 E. James E. Rogers Way, Tucson, Arizona 85721
[d]University of Arizona, Department of Surgery, 1501 N. Campbell Avenue, Tucson, Arizona 85724

Abstract. The accepted screening technique for colon cancer is white light endoscopy. While most abnormal growths (lesions) are detected by this method, a significant number are missed during colonoscopy, potentially resulting in advanced disease. Missed lesions are often flat and inconspicuous in color. A prototype ultraviolet spectral imager measuring autofluorescence (AF) and reflectance has been developed and applied in a study of 21 fresh human colon surgical specimens. Six excitation wavelengths from 280 to 440 nm and formulaic ratio imaging were utilized to increase lesion contrast and cause neoplasms to appear bright compared to normal tissue. It was found that in the subset of lesions which were most difficult to visualize in standard color photographs [low contrast lesions, (LCLs)] a ratio image (F340/F440) of AF images excited at 340 and 440 nm produced extraordinary images and was effective in about 70% of these difficult cases. Contrast may be due to increased levels of reduced nicotinamide adenine dinucleotide, increased hemoglobin absorption, and reduced signal from submucosal collagen. A second successful ratio image (R480/R555) combined two reflectance images to produce exceptional images especially in particular LCLs where F340/F440 was ineffective. The newly discovered ratio images can potentially improve detection rate in screening with a novel AF colonoscope.
[DOI: 10.1117/1.JBO.18.1.016005]

Keywords: endoscopy; fluorescence; medical imaging; multispectral imaging; reflectance; ultraviolet; colon; cancer; gastroenterology.

Paper 12458 received Jul. 17, 2012; revised manuscript received Nov. 14, 2012; accepted for publication Dec. 3, 2012; published online Jan. 4, 2013.

1 Introduction

White light colonoscopy is the preferred screening technique for colon cancer but fails to detect a significant number of polyps and flat neoplasms.[1–3] Improving the detection rate will help prevent incident cancers and decrease screening intervals and thus reduce the overall cost of colon cancer screening. Flat lesions, loosely defined as having a height less than half their width, are of special concern because they are more frequently cancerous than polypoid lesions,[4] and in a recent study, the prevalence of flat lesions was determined to be 9.4% of male veterans undergoing colonoscopy.[4] Indigo carmine chromoendoscopy increases the detection of flat neoplasms, but is too time consuming for use during screening exams in the U.S. where a high volume of colonoscopies must be performed under demanding time constraints.[3,4]

Identifying flat lesions using an endogenous contrast mechanism such as autofluorescence (AF) could provide benefits over chromoendoscopy by reducing exam time and eliminating dye toxicity concerns. AF image contrast in tissue is derived from the native tissue fluorophores [tryptophan, collagen, reduced nicotinamide adenine dinucleotide (NADH), flavin adenine dinucleotide (FAD)] as well as from the effects of absorption and scattering of other components (hemoglobin).[5] Spectroscopic AF studies comparing normal and neoplastic tissues have consistently noted reduced AF intensity from neoplasms. This general result was obtained in colon tissue at excitation wavelengths including 337,[6] 370,[7] and 442 nm.[8] Discrimination based on reduced AF intensity has put emphasis on correcting AF intensity measurements for variations in absorption, illumination intensity, and tissue surface morphology. It has also drawn attention to methods such as time-resolved AF imaging,[9,10] which largely avoids the confounding factors for intensity measurements but has its own drawbacks including instrumentation complexity and long acquisition times.

The correction of absorption and scattering effects in tissue AF images derives from a mathematical method used to remove such distortions from tissue AF spectra measured with a fiber optic probe.[11] That method relies on collection of both reflectance and AF spectra as well as knowledge of the tissue optical properties.[11] The simplified correction extended to AF imaging does not require knowledge of optical properties and is performed by dividing collected AF intensity at each emission wavelength by collected diffuse reflectance at the same wavelength.[12] Similarly, dividing an AF image by a cross-polarized reflectance image at the excitation wavelength has been shown to produce a ratio image corrected for variation in excitation-collection geometry and irregular tissue surface.[13,14]

Address all correspondence to: Urs Utzinger, University of Arizona, Department of Biomedical Engineering, 1127 E. James E. Rogers Way, Tucson, Arizona 85721. Tel: 520-621-5420; E-mail: utzinger@email.arizona.edu

0091-3286/2013/$25.00 © 2013 SPIE

Commercial AF endoscopes for the colon include the AFI system (Olympus Medical Systems, Tokyo, Japan) and PINPOINT system (Novadaq Technologies, Mississauga, Ontario, Canada; formerly the Onco-LIFE and LIFE-GI system, Xillix Technologies). The first developed was LIFE-GI[15] which illuminated tissue with blue light (400 to 450 nm) and measured both green AF (490 to 560 nm) and red AF (>630 nm). Later generations of LIFE-GI[16] have included simultaneous blue and red illumination and ceased collection of red AF in favor of red reflectance (>630 nm). The AFI system[17] illuminates with blue light (395 to 475 nm) and green light (540 to 560 nm) in succession and measures green/orange AF (490 to 625 nm) followed by green reflectance. Both of these commercial endoscopes electronically combine a blue-excited AF image and a reflectance image in a single pseudocolor image presented to the physician. Color differences in the pseudocolor composite image are used to signal the observer to the presence of a lesion. Contrast in images from these endoscopes is produced primarily by a loss of green AF in lesions and is perceived as a changed color ratio. Intensity artifacts due to geometrical shape of the specimen would be apparent in a single image; however, they are reduced in the pseudocolor image because the AF and reflectance images are affected by the same artifacts, preserving the color ratio of the resulting image. Several randomized trials comparing AF endoscopy in the colon to standard video endoscopy, narrow band imaging (NBI), or high resolution endoscopy have been published very recently. The outcomes of these studies have been mixed, with some indicating these AF endoscopes can reduce polyp miss rate[18–20] and others showing no significant improvement of AF over other technologies.[21–23]

Other studies have also combined tissue AF images at multiple wavelengths or an AF image and diffuse reflectance image. For example, AF-based ratio images in the near infrared were used to highlight carcinoma in resected breast tissue.[24] Ratio images in the ultraviolet were found to enhance structure visibility in microscopic images of human esophagus.[25] A third study used AF ratio images to highlight adenomatous regions in cross sections of excised colonic polyps.[26] Still others have demonstrated the use of AF ratio images microscopically for monitoring cell metabolism and differentiating cancerous tissue.[27–29]

Previously, we reported early results from an AF imaging study of fresh surgical specimens of human colon.[30] In this paper we expand on that study and describe in detail the development of a prototype multispectral imager with ultraviolet C (UVC) excitation capability. Analyzing spectral images of cancer and polyps, we experiment with novel ratio images, some employing multiplication, addition, and three or more image types. Using a combination of quantitative and qualitative measures, we identify the most effective ratio images in terms of lesion contrast, predicting that an exceptional contrast in this study will translate to an increased detection of flat lesions in the clinical setting. Finally, we compare our formulated ratio images to commercial AF technology and discuss the potential of this AF method for incorporation in an advanced endoscope for use in colorectal cancer screening.

2 Materials and Methods

2.1 *Instrumentation*

The imaging system used to collect both AF and reflectance images was a prototype developed in our laboratory (Fig. 1). The spectral imager with extended UV range (illumination from 260 to 650 nm and detection from 340 to 650 nm) and fixed working distance of 25 cm was used to collect macroscopic tissue images, 4 cm^2, at the surface of resected tissues. The light source was a xenon arc lamp system (300 W, Lambda LS, Sutter Instruments, Novato, California) with a built-in ten-position filter wheel. Use of a full-spectrum bulb allowed significant output in the 260 to 300 nm range but necessitated a custom UV cold mirror (Chroma, Bellows Falls, Vermont) with high reflectance over the same range and an ozone filter (Oriel Instruments, Irvine, California). A filter wheel controller (Lambda 10–3, Sutter Instruments, Novato, California) provided automated selection of both illumination and detection wavelengths. A custom quartz fiber bundle (FiberTech Optica, Ontario, Canada) delivered illumination to the specimen and included a feedback fiber for monitoring lamp power fluctuations. The thermoelectrically cooled, UV-enhanced camera (PhotonMAX:512B, Princeton Instruments, Trenton, New Jersey) with intensified CCD (e2v CCD97B, e2v technologies, Chelmsford, England) was mounted on a rigid mobile arm and equipped with a color-corrected UV imaging lens ($f/3.5$, $f = 63$ mm, Resolve Optics, Chesham, United Kingdom). A second ten-position filter wheel was mounted directly in front of the imaging lens. A LabVIEW (National Instruments, Austin, Texas) interface was developed in our laboratory and used to control the two filter wheels, single mechanical shutter, and image acquisition. Automation via scripting allowed sequential capture of 27 different images of interest (and their corresponding dark frames) in about 90 seconds.

All illumination was narrowband (~20 nm full-width-half-maximum) and accomplished with bandpass interference filters, whereas on the imaging side, longpass filters were used exclusively. Longpass emission filters were selected to enable collection of weak AF using shortest exposure times. Illumination for diffuse reflectance images was passed through a removable UV polarizer (UV1 precision linear, Meadowlark Optics, Frederick, Colorado) and collected through a second UV

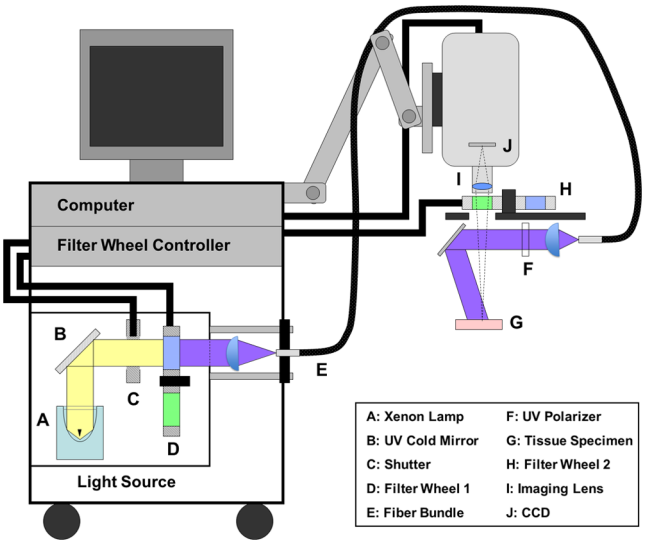

Fig. 1 Prototype multispectral imager. A cart-based system with camera mounted on mobile arm was customized to allow both UV and visible imaging and to excite fluorescence with wavelengths as short as 270 nm. Specialized components included a full-spectrum xenon lamp, custom UV cold mirror (high reflectance 270 to 650 nm), quartz optics, and removable UV polarizers.

Table 1 Autofluorescence images with names specifying excitation wavelength.

Name	Emission (nm)	Target fluorophore	(Other)
F280	345–410	Tryptophan	(Pyridoxine)
F320	375–410	Collagen	(Pyridoxine)
F340	410–500	NADH	(Collagen, Elastin)
F370	410–500	Collagen	(NADH, Elastin)
F400	600–655	Porphyrins	
F440	500–600	FAD	(Collagen)

polarizer mounted in the emission filter wheel. AF contribution to the reflectance images was neglected because it is typically 1000 times less than reflectance.

The excitation wavelengths and emission bands of the AF images were chosen to target native fluorophores (tryptophan, collagen, NADH, FAD, porphyrins) whose concentrations and distributions may change with disease state. Table 1 defines six AF images of interest (F280, F320, F340, F370, F400, and F440), named according to excitation wavelength, and also lists the targeted tissue fluorophores. Excitation and emission spectra of several of these fluorophores are known to overlap, which leads to influence of nontargeted fluorophores in some images. Each of the AF images is formed by subtraction of two different longpass-filtered images. For example, the 320-nm-excited AF image, F320, is formed by subtracting 410-nm longpass image from 375-nm longpass image to create an AF image associated largely with collagen. The six diffuse reflectance images collected are referred to as R370, R400, R415, R440, R480, and R555 where the names specify center wavelength of narrow band illumination. The crossed polarization of these images greatly suppresses specular reflections.

2.2 *Instrument Verification*

Performance of the imaging system was characterized prior to the clinical study. First, a spectrophotometer (Cary 5, Varian Inc., Palo Alto, California) was used to obtain transmission spectra for all system optical filters. Bandpass excitation filters all possessed out-of-band attenuation four to five orders of magnitude greater than in-band. All the longpass emission filters showed five orders of magnitude greater attenuation below the cut-on wavelengths.

Illumination exiting the fiber bundle was measured using a portable spectrophotometer (USB2000, Ocean Optics, Dunedin, Florida). Illumination at 320, 340, and 440 nm revealed no measurable out-of-band light (indicating out-of-band illumination at least 5 orders of magnitude weaker than in-band). Often two filters were stacked to achieve this desired condition. The 280 nm illumination had no measurable out-of-band light besides a spectral feature at 825 nm which was 4.4 orders of magnitude below peak intensity. Though weak, this near infrared light had potential to influence the long pass filtered images of weak fluorescence collected with our camera. Therefore, we additionally placed a shortpass filter (FF01-680/SP, high transmission 345 to 655 nm, Semrock Inc., Rochester, New York) permanently in front of the camera's imaging lens.

In order to estimate the maximum possible influence of reflected excitation light in tissue AF images, a cuvette of Al_2O_3 powder (nonfluorescent, high-reflectance material) was imaged side-by-side with a finger of one of the investigators. Ratios were calculated of AF image intensity at the finger to AF image intensity at the Al_2O_3 powder. For images F280, F320, F340, F400, and F440 the respective ratios were 19.6, 10.1, 13.7, 5.8, and 8.4. Therefore the influence of reflected light leakage in an F280 image is less than 5%, while in F400 its influence may reach 15%. This confirmed that the AF images would be dominated by fluorescence.

2.3 *Clinical Measurements*

The imaging study was approved by the institutional review board of the University of Arizona Medical Center. Prior informed consent was obtained from patients undergoing colonic resection for clinical indications. Colon specimens were obtained fresh from surgery and imaged thirty to 60 min after excision in a separate darkened room in the same building. Specimens were positioned with the luminal surface facing up and rinsed with saline to remove any blood or stool. Images were composed to include the edge of the lesion allowing comparison with the surrounding normal mucosa in a single photograph. Following spectral imaging, color reference images of specimens were collected using a standard digital SLR camera. Histopathology of each specimen was obtained and used as the gold standard for diagnosis.

Steps were taken to ensure that clinical AF images could be compared quantitatively. During each tissue imaging sequence, optical power meter readings were collected via the feedback branch of the bifurcated optical fiber bundle. Upon completion of specimen imaging, power from the feedback fiber was measured again, and a secondary reading was collected at the specimen imaging location. Solid fluorescence standards (Starna Ltd., Hainault, United Kingdom) including naphthalene, ovalene, tetraphenylbutadiene, and compound 610 were also imaged and reflectance images taken of a flat Spectralon target (Labsphere, North Sutton, New Hampshire).

The study has thus far included imaging of specimens from 30 patients as detailed in Table 2. Twenty-one of 30 specimens from colorectal surgery involved adenocarcinoma (cancer). The low number of adenomas (adenomatous polyps) acquired reflects that adenomas are precursor lesions removed by surgery only when colonoscopic removal is not feasible. To reduce influence of factors not being studied, nine specimens were omitted from the analysis. Factors leading to omission from quantitative AF analysis included highly ulcerative (bloody)

Table 2 Study specimens imaged and documentation of exclusions.

	Specimens	Adenocarcinoma	Adenoma	Other
Overall	30	21	7	2
Final #s	21[a]	14	7	0

[a]Excluded from quantitative analysis were: highly ulcerative lesions ($n = 3$), tissues from patients with chemo/radiation treatment ($n = 3$), cancers not originating in colon ($n = 1$), cases with equipment issues ($n = 2$)

lesions, lesions that were subjected previously to chemotherapy or radiation treatment, cancers not originating in the colon, and equipment issues.

2.4 *Image Processing and Analysis*

Raw images were processed using MATLAB (The MathWorks, Natick, Massachusetts). Dark current and room light were compensated by subtracting corresponding dark frames (illumination blocked with shutter). Flat fielding was performed through division by normalized images of a white standard. Source power variation was compensated through division by single correction factors representing relative power readings on date of imaging. Integration times were corrected for as appropriate using a multiplicative factor.

To facilitate quantitative image analysis, regions of interest (ROIs) were selected manually for each specimen with input from a physician experienced in colonoscopy. Circular ROIs were traced over the F280 specimen image in MATLAB while referencing a color reflectance image as illustrated in Fig. 2. This task was performed while blinded to all other image types. A set of one to three ROIs was chosen to represent the lesion and a separate set chosen to represent the most normal appearing tissue. Both ROI sets were saved and later applied in analysis of the AF, reflectance, and ratio images. In cases where two or more fields of view of a specimen had been imaged, a single image set involving just one field of view was selected by observing only the color reference images.

2.5 *Quantitative Image Analysis*

Two different metrics were employed to quantify lesion visibility and evaluate the various ratio and nonratio images. The first metric [Eq. (1)] is based on the well-known Weber contrast which takes the form $(I_A - I_B)/I_B$. The second metric [Eq. (2)] was developed and optimized by the authors. In Eq. (1), I_{Lesion} and I_{Normal} are the mean pixel intensities inside the respective ROIs of a specimen image. Similarly, in Eq. (2), $I_{\text{Lesion},75\%}$ and $I_{\text{Normal},75\%}$ are the 75th percentile pixel intensities inside respective ROIs of the specimen image. Furthermore, $\sigma_{L,N}$ is the pooled standard deviation as calculated from the individual standard deviations, σ_L and σ_N, of the pixel intensities inside the respective ROIs.

$$C_{\text{Weber}} = \frac{I_{\text{Lesion}} - I_{\text{Normal}}}{I_{\text{Normal}}} \tag{1}$$

$$C_{\text{Opt}} = \frac{|I_{\text{Lesion},75\%} - I_{\text{Normal},75\%}|}{\sigma_{L,N}} \quad \text{where } \sigma_{L,N} = \sqrt{\frac{(\sigma_L^2 + \sigma_N^2)}{2}}. \tag{2}$$

The optimized contrast metric [Eq. (2)] was formulated because the Weber contrast favored ratio images of the form $1/(A * B)$ over those of forms $A/(A + B)$ and A/B. Ratios of the form $1/(A * B)$ tended to greatly magnify the numerator of Eq. (1), but also greatly increased the spread of ROI pixel intensities, limiting observed contrast improvement. The optimized metric was also designed to account for the standard deviation, or spread, of the ROI pixel intensities. The 75th percentile intensity was selected as a more consistent measure of ROI intensity in the ratio images (where highly asymmetric distributions of pixel intensities were observed).

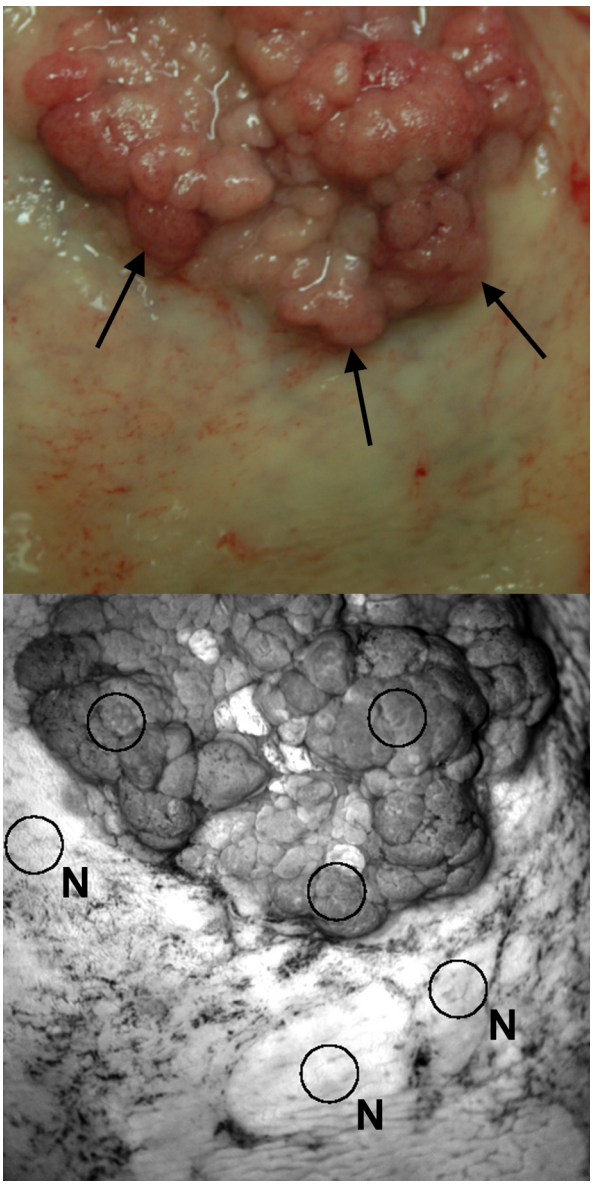

Fig. 2 Illustration of region of interest (ROI) assignment. In the color reference image taken with digital SLR camera, the arrows indicate the edge of a raised adenocarcinoma. The grayscale image is an F280 image with three circular ROIs labeled N to designate normal and three unmarked circular ROIs representing the lesion. Care was taken during ROI placement to avoid surface vasculature or blood.

To aid in evaluation of the two contrast metrics, authors T.R. and U.U. determined visual contrast scores for each of the formulated ratio images (observing them side by side, one specimen at time). A visual score from one (no useful contrast) to four (best lesion contrast) was assigned to each formulaic ratio image for each of nine specimens in a study subgroup. The most effective contrast metric was taken to be the one with highest correlation to the visual scores of lesion contrast.

2.6 *Image Display and Visual Analysis*

For selection of the most useful formulaic ratio images, side-by-side visual comparison was effective but heavily dependent on

comparable display of various ratio image types. Division by low pixel values and multiplications produced a wide range of ratio image intensities and a variety of distributions making consistent display a nontrivial task. Following calculation of ratio image intensities, we found it necessary to eliminate the very highest pixel intensities by observing a collective histogram of pixel intensities from all ratio images of the same type and setting all values above a threshold to that threshold level.

Three general methods were used to scale image data for display in grayscale on a monitor. In the "fixed" scaling method (similar to the initial thresholding step applied to all ratio images), the intensities from a large number of images of the same type were observed collectively and suitable minimum and maximum intensity levels chosen to set the low and high ends of the display range. Scaling was "fixed" because every image of the same type was scaled identically. Fixed scaling was appropriate for the AF and reflectance images because the overall variation in intensity values was low. The second method, "autoscaling," is an adaptive method because new minimum and maximum intensity levels are chosen for each image. This ensures every image will have the same amount of completely white and completely black pixels and may alternately be called saturation scaling. The third method, "histogram equalization" is an adaptive method which not only determines appropriate maximum and minimum intensity levels, but also performs the scaling nonlinearly such that the image's intensity distribution resembles a preselected shape. The result is an image more vibrant but also less quantitative. In scaling each formulaic ratio image for display, either autoscaling or histogram equalization was preferred. As part of all three scaling methods, 1% of intensities were intentionally saturated at both the high and low ends to increase contrast with little loss of information. Scaling methods were applied solely to improve visual appearance of displayed images; all quantitative calculations of contrast were carried out using unscaled image data.

For formal visual analysis, various formulaic ratio images of the same colon specimen were displayed side-by-side in a tiled image. Each ratio image was scaled for display using the preferred method for the specific ratio image type. The identity of each tiled ratio image was concealed from the observers. Visual image scores were individually recorded by seven persons (T.R., B.B., L.G., N.R., U.U., R.L., B.B.) familiar with the project including two physicians (one of these an experienced colonoscopist) and two engineering faculty. Attending researchers were asked to indicate in each ratio image whether the lesion contrast was "adequate" for identification and also to note whether the image could be considered "exceptional." This process was repeated for all specimens.

2.7 *Formulaic Ratio Images*

We formulated over thirty novel ratio images while aiming to maximize lesion visibility and brighten lesions in comparison to surrounding normal tissue. Names were assigned to trial ratio images sequentially (R1, R2, R3, etc.). A select group of the attempted ratio images is presented in Table 3. Many formulas incorporate three or more images as well as a multiplication and/or an addition operation. For the ratios that include an addition operation, all images involved were verified to possess similar average brightness or adjusted by a constant factor before ratio image calculation. As a general rule, AF images expected to display increased lesion intensity (F280, F340) were placed in the numerator of ratios, while AF images expected to display decreased lesion intensity (F320, F440) were placed in the denominator. In some cases, simple mathematical inversion was performed (R10, R20). Ratio images related to our previously published redox ratio[31] are R15 and R27.

Table 3 Select group of trial formulaic ratio images. (F440red refers to an AF image excited at 440 nm with emission collected from 600 to 655 nm.)

$R7 = \frac{1}{F440 * F320}$	$R24 = \frac{1}{R555 + F440}$
$R10 = \frac{1}{F440}$	$R25 = \frac{1}{R555 * F440}$
$R15 = \frac{F340}{F340 + F440}$	$R27 = \frac{F340}{F440}$
$R20 = \frac{1}{R555}$	$R30 = \frac{R480}{R555}$
$R23 = \frac{1}{F440red + F440}$	

2.8 *Ratio Image Simulation of Commercial AF Endoscope Images*

To compare our formulated ratio images to existing technology, we created ratio images (in grayscale) approximating the color contrasts of two different commercial AF colonoscopes. Ratio image R21 (=F440red/F440) is modeled after the red/green ratio (ratio of red AF to green AF) described by Zeng et al. as determining color in the LIFE-GI system.[15] Ratio image R22 (=R555/F440) simulates the G/R ratio (ratio of green AF to green reflectance) described by Aihara et al. as approximating color tone in the AFI system.[32] Intensity differences seen in grayscale images R21 and R22 estimate the color differences seen on each system's pseudocolor display and used to identify lesions. The Onco-LIFE system images could not be simulated because a red reflectance image is required and was not collected as part of this study.

3 Results

The mean lesion contrast of AF and reflectance intensity images from the clinical study is displayed in Fig. 3 with specimens stratified by histology. For all image types, the regions representing the lesions produced lower image intensities than the regions of surrounding normal mucosa. Adenocarcinomas were easier to identify than adenomas in both AF and reflectance images, though it should be noted that the majority of lesions in the adenocarcinoma group were well-established masses with increased vascularity. F440 produced the highest mean contrast in the adenocarcinomas studied yet displayed no statistically significant increase in contrast over image types R400, R415, R555, F320, and F370 (T-test, $p > 0.05$). In the adenoma group, the advantage of F440 was even less significant with only F280, F340, and F400 judged lower contrast by T-test ($p < 0.05$). The influence of hemoglobin on narrowband reflectance images is evident in the right side of Fig. 3 where the plotted contrast resembles the absorption spectrum of hemoglobin (primary peaks between 400 and 440 nm and a local maximum near 550 nm).

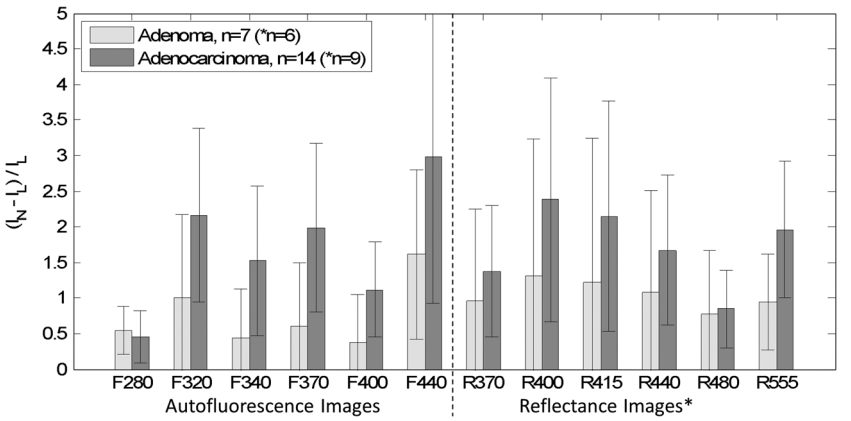

Fig. 3 Lesion contrast results for adenomas ($n = 7$) and adenocarcinomas ($n = 14$) in various image types. (Reflectance images were available only for the final six adenomas and nine adenocarcinomas.) This plot specifies the mean Weber contrasts and standard deviations for each image type. Because $I_N > I_L$ in these images, lesion and normal intensities were interchanged in Eq. (1). Image F440 displayed the most lesion contrast for both adenomas and adenocarcinomas, but its performance was statistically similar to several other image types.

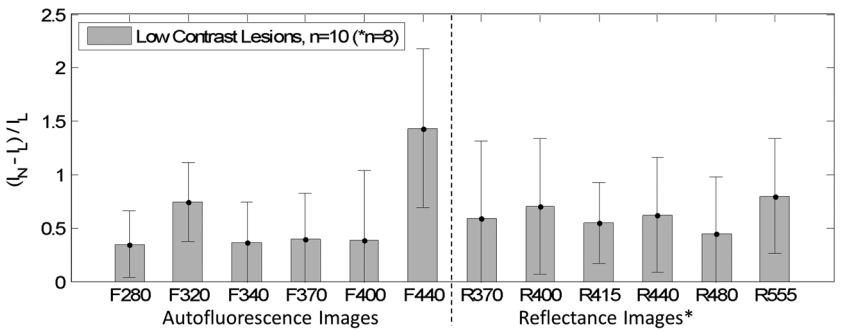

Fig. 4 Lesion contrast results for the low contrast lesion specimen subgroup whose members were all difficult to visualize in RGB color photographs taken with a standard digital camera. This group included adenomas ($n = 6$) and adenocarcinomas ($n = 4$). (Reflectance images were available only for the final five adenomas and three adenocarcinomas.) This plot specifies the mean Weber contrasts and standard deviations for each image type. Because $I_N > I_L$ in these images, lesion and normal intensities were interchanged in Eq. (1). Image F440 displays greatest contrast, and the increase is statistically significant (T-test, $p < 0.05$) compared to all of the other image types.

Because the goal of this study was to develop a useful imaging technique for flat and nearly invisible lesions, we analyzed a subgroup of specimens that were most difficult to identify in the RGB color photographs taken with a standard digital camera. We refer to these as "low contrast lesions," or LCLs. This subgroup included six adenomas and four adenocarcinomas. Plotting the mean Weber contrast of this subgroup (Fig. 4) reveals an advantage for AF image F440 in identifying LCLs. The increase in contrast of F440 over all the other image types was confirmed by T-test comparisons ($p < 0.05$).

Even with the highest contrast image type (F440), roughly half of all LCLs could not be well visualized. We also observed interference in this image type from blood and geometrical features (folds) which appear dark and could reduce specificity. Formulaic ratio images were sought to gain high visualization of more of the LCLs. Two contrast metrics proposed to aid in evaluating ratio images were tested by plotting the results of each metric versus visual contrast scores and performing linear fits to the data (not shown). Our optimized contrast metric [Eq. (2)] achieved a higher correlation than the Weber contrast [Eq. (1)], with its linear fit yielding an R-squared of 0.58 as compared to 0.21.

Narrowing the pool of ratio images was achieved by first grouping them based on visual similarity. We identified six such groups as well as four ratios seemingly unique to the others. Equation 2 was then used to calculate lesion contrast for all ratio images of all study specimens. The mean optimized contrast metric score and standard deviation of each ratio image type were compared stratifying adenocarcinoma, adenoma, and low contrast lesion. Formulaic ratio images with a high contrast performance in one or more of these subgroups were chosen for additional visual analysis. Also, effort was made to retain at least one ratio from each of the six groups of similar visual impression. This approach resulted in nine formulaic ratio images with high diagnostic potential (Table 3).

In selecting the best high contrast ratio images, we focused on visual analysis. The appropriate method of scaling each formulaic ratio image was determined by observing visual results on images of all specimens. Examples of the effects of autoscaling and histogram equalization are illustrated in Fig. 5. The better display scaling choice was found to correlate with the mathematical form of each ratio. Ratio images such as R27 and R30, having the form A/B and small ranges of intensities, were displayed effectively with autoscaling. This method was slightly less effective for ratios of the form $1/A$ and $1/(A + B)$ but still the preferred choice. For ratio image R7 of the form $1/(A * B)$, histogram equalization was the preferred scaling method for display. When autoscaled, this ratio image

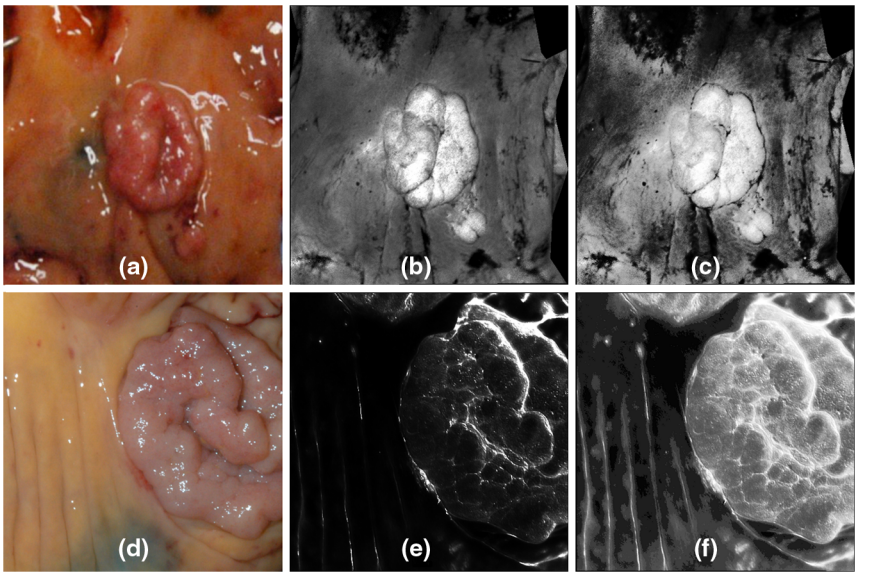

Fig. 5 The effects of autoscaling and histogram equalization on visualization of formulated ratio images are shown. (a) Standard color photo of an adenoma taken with digital SLR camera. (b) Autoscaled R27 ratio image. (c) Histogram equalized R27 ratio image. (d) An adenoma from a different specimen imaged by digital SLR camera. (e) Autoscaled R7 ratio image. (f) Histogram equalized R7 ratio image. Images (a), (b), and (c) demonstrate that autoscaling of ratio image R27 is more effective than histogram equalization, while (d), (e), and (f) show the benefit of histogram equalization for ratio image R7. Tattoo ink applied prior to excision causes dark color artifacts in images a (immediately left of polyp) and d (bottom center of image).

frequently became dark because a small but substantial percentage of pixel intensities were much higher than any others in the image. For ratio image R15, which has the form $A/(A+B)$, histogram equalization was preferred because autoscaling produced a washed out appearance.

Visual analysis of the selected ratio images (Table 3) was conducted by tiling the nine images of a single specimen on a large display, recording visual scores, and repeating the process for all specimens. Results were stratified by LCL versus nonLCL and are displayed in Fig. 6 as percentages of imaged specimens for which a majority of observers deemed the image "adequate" for lesion identification. As narrowband reflectance imaging was not available for the first six specimens in our study, ratio images R20, R24, R25, and R30 were not available for six out of twenty-one specimens. However, this is accounted for by plotting results as percentages of specimens imaged. The data demonstrate that image R10 (1/F440), regardless of specimen group, was never exceeded in its ability to produce adequate contrast. R23 images were nearly identical to R10 in appearance and visual performance. Ratio R27 (F340/F440) frequently produced exceptional images of LCLs as well as adequate performance on nearly the same percentage of LCLs as R10. R30 (R480/R555) produced many exceptional images in both lesion subgroups but produced fewer adequate images when compared to R10. A second stratification (adenoma versus adenocarcinoma, not shown) produced highly similar results due to the majority of the LCLs being adenomas and majority of nonLCLs being adenocarcinomas. Figure 7 provides examples of R27 ratio images for three specimens classified as low contrast lesions. Remarkable lesion contrast is observed for this fluorescence based ratio. Ratio image R30 was effective especially in the more obvious lesions (nonLCLs) but also produced exceptional contrast for a few of the lesions most difficult to identify with white light. Figure 8 presents color photographs and R30 ratio images for three specimens. Two of these three

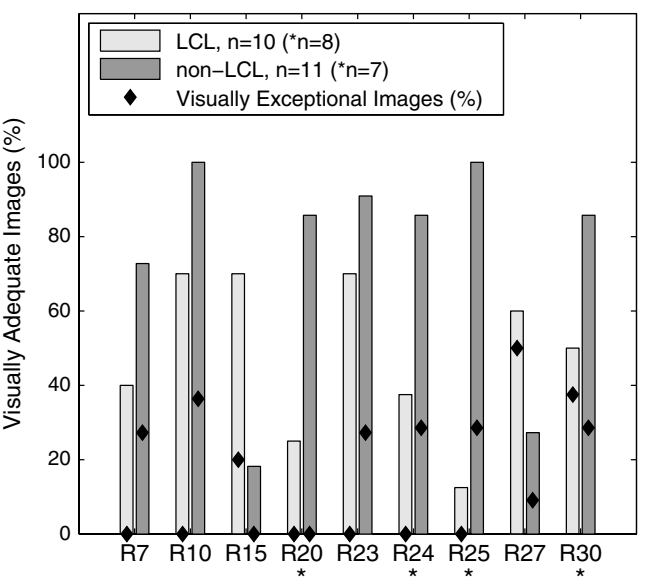

Fig. 6 Visually assessed performance of formulaic ratio images. Bars represent the percentage of specimen images for which a majority of observers (four of seven) deemed the image "adequate" for lesion identification. Diamonds represent the percentage of specimen images for which at least three of seven observers deemed the image "exceptional." Results are stratified by low contrast lesion (LCL) status of specimens. Ratio images of LCLs generally were less effective than images of non-LCLs (with the exceptions of R15 and R27). R10 produced the highest percentage of adequate images, but R27 and R30 exceled in the LCL group by producing the highest percentage of exceptional images. When data was alternately stratified by histology, visual performance was nearly identical to the graph shown here; performance on adenomas was similar to LCLs and performance on adenocarcinomas was similar to non-LCLs.

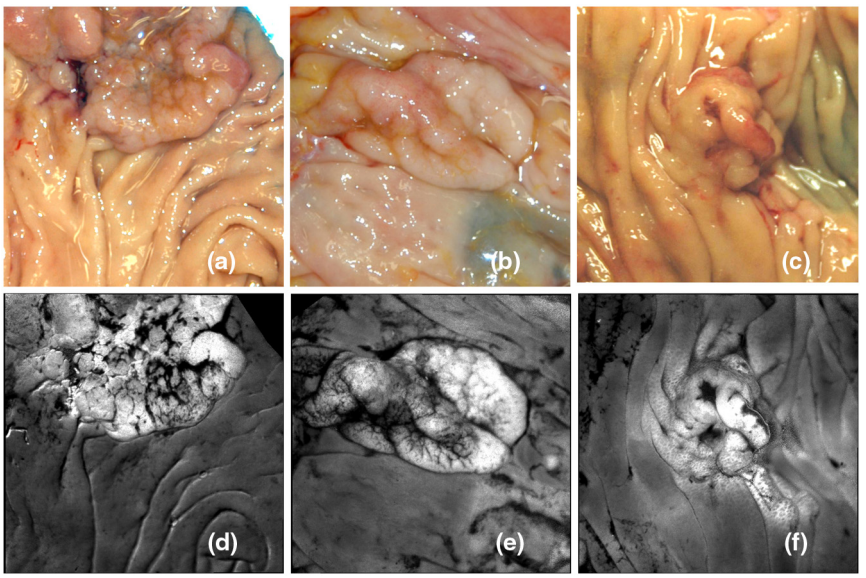

Fig. 7 Low contrast lesion examples from resected specimens of three patients. (a) Tubulovillous adenoma, (b) Serrated adenoma, (c) Adenocarcinoma. Grayscale ratio images R27 = F340/F440 presented in (d)–(f) highlight the lesions which are nonevident in color photos (a)–(c). Dark regions in the lower right corner of image b and center right of image c are caused by tattoo ink applied prior to specimen excision for marking purpose.

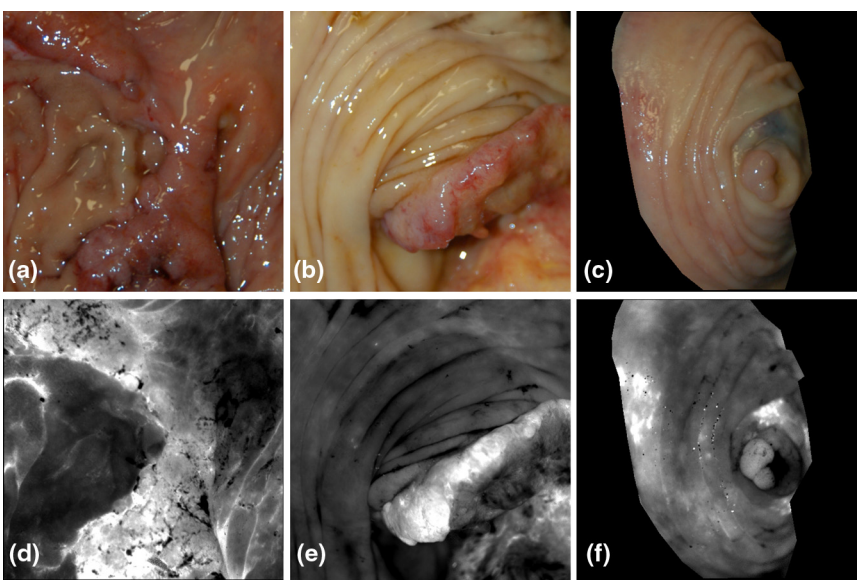

Fig. 8 Three specimens and corresponding R30 = R480/R555 ratio images in grayscale. (a) Adenocarcinoma, (b) Adenocarcinoma, (c) Tubular adenoma. Specimens a and c were low contrast lesions. The smaller specimen shown in (c) and (f) is masked to show only tissue. The brightest regions of (d) and (e) correspond to lesions. In (f) the brightest regions correspond to inflamed mucosa (left) and tattoo ink (right) used previously to mark the lesion location. In (f) the 6-mm polyp is visible directly below the bright tattoo ink.

(a and c) could be adequately visualized neither by ratio image R27 nor by R10.

To compare the most successful ratio images to existing AF endoscope technology, a second visual analysis was performed using the same procedure as the first but including ratio images R21 simulating the LIFE-GI system and R22 simulating the AFI system. To reduce potential bias, the eight persons participating were blinded to the identity of the images being evaluated. Results are presented in Fig. 9. An advantage is seen for R27 in percentage of LCLs visualized both exceptionally and adequately. The data also demonstrate that performance can be further improved using R27 and R30 in parallel due to complementary ability of the two ratio image types. Figure 10 shows four images of the same large flat polyp (tubulovillous adenoma) of a proximal colon specimen. The lesion was difficult to visualize in white light (color photograph). Each ratio image in the figure was autoscaled for display, saturating only small fractions of each image. The ratio images simulating color contrasts of the LIFE-GI and AFI colonoscope systems display considerably less contrast than the newly discovered ratio R27. The contrasts calculated with Eq. (2) were −0.80, 3.17, and 4.52, respectively for figure images b, c, and d. Compare these results to the mean contrasts calculated for all 10 LCLs (1.86, 2.18, and 3.30, respectively), and we see

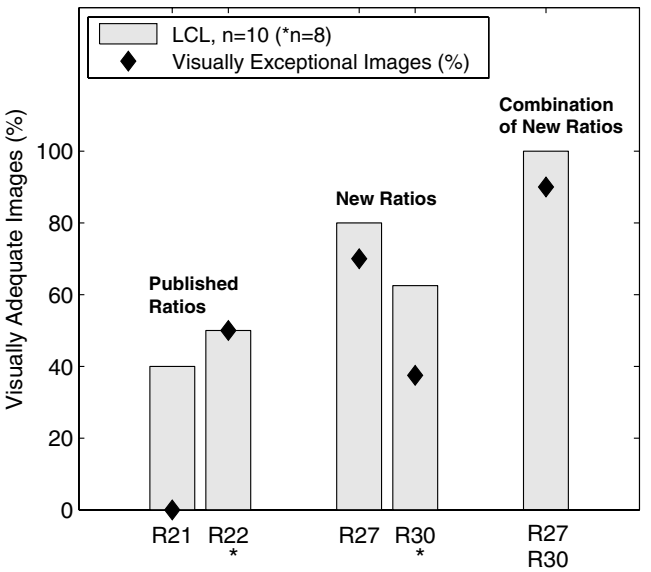

Fig. 9 Visually assessed performance of formulated ratio images compared to existing technology. Ratio image R21 = F440red/F440 approximates the red/green ratio used for polyp discrimination by LIFE-GI (Zeng, 1998). Image R22 = R555/F440 approximates the published G/R ratio used by the AFI system (Aihara, 2009). Bars represent the percentage of low contrast lesion images for which the ratio image was deemed "adequate" for lesion identification by at least four of eight observers. Diamonds represent the percentage of specimen images for which the ratio image was deemed "exceptional" by three or more of eight observers. The rightmost bar indicates the performance that might be achieved using R27 and R30 in parallel.

a trend of improvement (51%) using R27. A T-test on this data to determine the significance of the increase in all LCLs yields a p-value of 0.24 indicating that further data collection is warranted.

4 Discussion and Conclusions

In this study, we created formulaic ratio images which improve lesion contrast by incorporating signals attributed to different fluorophores and also reduce geometrical effects which distort measured AF intensity. We confirmed that the green fluorescence image commercialized as the basis for the LIFE systems[15] is effective at producing adequate lesion contrast in most of our samples. However, we found that for viewing low contrast lesions (LCLs), the most useful formulaic ratio image combined an F340 image with an F440 image. At the 340 nm excitation wavelength, both collagen and NADH contribute to colon AF. A previous study found that in normal colon tissue excited at this wavelength, the AF of NADH was overshadowed by signal from submucosal collagen.[6] However, in adenomatous polyps and adenocarcinoma the influence of NADH on the measured AF signal was pronounced and sometimes exceeded that of collagen.[6] In our study, the F340 image showed increased AF intensity in some of the low contrast lesions (data not shown) leading to improvement of the formulaic ratio image R27 = F340/F440. Though not experimentally proven, we partially attribute the gains in lesion contrast to increases in lesion NADH fluorescence as captured by the F340 images. This explanation is further supported by the finding that NADH fluorescence increases in neoplastic tissues,[33] whereas collagen AF is known to decrease.[6]

The second image type used in the most successful formulaic ratio image was the AF image F440. The dominant contribution to colon AF signal at 440-nm excitation has been shown to come from collagen in the submucosa rather than mucosal FAD.[8] The pronounced AF decrease observed in adenomas and adenocarcinomas excited at this wavelength has been attributed to both mucosal thickening and increased mucosal blood content.[8] Our visual analysis of formulaic ratio images confirmed 440 nm as the key excitation wavelength for lesion viewing, as R10 = 1/F440 produced the greatest percentage of useful images. Our study also yielded a combination of two reflectance wavelengths that is very effective in highlighting many lesions. The ratio image R30 = R480/R555 incorporates green light which is sensitive to hemoglobin absorption and blue-green light which is relatively insensitive to hemoglobin absorption. In this ratio image R555 provided most of the contrast (see Fig. 4) and R480 served as a reference image correcting effects of geometry. This observation indicates that lesion contrast in R30 is likely driven by hemoglobin concentration. R27 produced exceptional contrast in 50 to 70% of LCLs (the number varied slightly with observer group), whereas ratio image R30 displayed exceptional contrast in about 40% of the LCLs including two that were not well visible in R27. R30 also produced exceptional images in about 40% of nonLCLs and was superior to R27 in that group. The complementary performances of R27 and R30 indicate that while lesion contrast in R30 is enhanced by hemoglobin presence, lesion contrast in R27 may be inhibited by it.

In the process of discovering effective formulaic ratio images, we have also drawn important conclusions about ratio imaging in general. We tested forms of formulaic ratio images involving two, three, and four different image types. Ratios such as A/B, $1/(A+B)$, $A/(A+B)$, $C/(A+B)$, $1/(A*B)$, $C/(A*B)$, $(C*D)/(A*B)$, and $(C+D)/(A+B)$ were tested as well as simple inversions $(1/A)$ which produce a

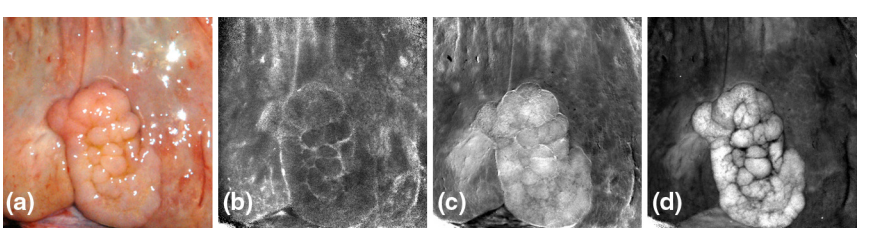

Fig. 10 Comparison of existing technology to formulaic ratio image R27 in a large flat polyp of the proximal colon. A tubulovillous adenoma is shown in (a) digital SLR photo, (b) ratio image R21 = F440red/F440 simulating LIFE-GI system, (c) ratio image R22 = R555/F440 simulating AFI system, and (d) ratio image R27 = F340/F440. For this specimen the contrasts calculated with Eq. (2) were (b) −0.80, (c) 3.17, and (d) 4.52. In this example R21 produces little contrast, R22 some useful contrast, and R27 produces an exceptional result clearly defining the flat lesion. If all ten low contrast lesions are considered, the mean calculated contrasts obtained are 1.86 for R21, 2.18 for R22, and 3.30 for R27.

complementary image. Ratio images such as $1/(A*B)$, $1/(A+B)$, $1/A$, and $C/(A*B)$ which had more components in the denominator of the formula than in the numerator produced images of very high contrast when scaled properly for display. However, they also highlighted the darkened features of the AF and reflectance images, indiscriminately emphasizing both lesions and less important features like tissue folds. The formulaic ratio images of form A/B appeared to better compensate for geometrical effects and put emphasis on the behavior of the underlying fluorophores. This is in agreement with the observation of Zeng et al., that a second image may be used in an endoscope as a reference image to mitigate geometrical effects.[15]

In building the prototype imager, emphasis was given to UV imaging capability and ability to illuminate in the lesser explored 260 to 320 nm wavelength range. Despite previous findings of increased 280-nm-excited AF from cells isolated from colonic adenocarcinoma,[30] such an increase was not observed here in bulk tissue. Rather, both adenocarcinomas and adenomas excited with 280-nm light displayed slight reductions in AF compared to normal mucosa. As neoplasms are known to be hypervascular, the reductions in observed AF may be due to increased hemoglobin absorption. The F280 images attributed primarily to tryptophan AF were notable for their revelation of the smallest and sharpest surface features due to the minimal penetration depth of the illumination wavelength. Ratio images involving F280 were found less useful for identifying lesions than certain others not including F280.

As part of our analysis we also simulated contrast of two commercial AF colonoscopes and found that R27 produced 51% greater mean lesion contrast, a 40% increase in exceptional images of LCLs, and a 60% increase in adequate images of LCLs (Fig. 9). The simulation ratio image R22 = R555/F440 representing the AFI system from Olympus resulted in relatively less mean contrast because F440 and R555 often produced similar images with one partially canceling the contribution of the other. The lower performance could be due in part to the *ex vivo* nature of this study which can lead to additional accumulation of blood in the tissue due to trauma induced during surgery.[6] The simulation ratio image R21 = F440red/F440 representing the former LIFE-GI system of Xillix performed least effectively. The limited range of our F440red image (600 to 655 nm instead of 630 to 750 nm) may have limited the accuracy of the simulation ratio.

While it is important to note that the AF of a tissue *in vivo* and after its resection are different, the changes observed in surgical specimens are minimized by prompt measurement following resection. In a study of colon AF, the NADH signal from resected adenomatous polyps was found to decay by one half every 118 minutes, while signals from collagen and FAD were observed unchanged.[6] Specimens in the current study were imaged 30 to 60 min after resection which corresponds to a 16% to 30% reduction in NADH AF. AF signals from the extracellular matrix (collagen) and tryptophan are not expected to change, as they are less susceptible to oxidation. Future lesion contrast obtained *in vivo* with F340/F440 ratio images may improve over observations from this study, assuming that NADH AF decays more quickly in neoplasms (following resection) than in surrounding normal mucosa.

The formulaic ratio imaging method is an extension of existing AF imaging such as implemented in Olympus' endoscopic AFI system.[34] The primary differences, which present some endoscope design challenges, are our use of UV illumination and narrowband reflected light images. The 340 nm illumination used by ratio image R27 requires a UV source and UV transparent fiber bundle for light delivery adding some expense to the system, but imaging and coupling optics can be fabricated from an economy glass such as N-BK7 which transmits well down to 340 nm. UV mutagenicity must be considered for *in vivo* application, and it is therefore imperative that the endoscope possess good collection efficiency to minimize UV exposure. Miniature optics with an N.A. of 0.2 will increase the collection N.A. of the endoscope by a factor of five compared with the study imager. Rapid illumination wavelength switching, <2 ms, can be achieved with filter based commercially available systems employing dual scanning galvanometers. Ratio images must be calculated and scaled for display in real time, likely on a split screen next to white light images.

UV illumination also necessitates the establishment of safety thresholds for exposure which do not currently exist for the colon. Prior to clinical research in humans, exposure safety at 340 nm must be studied in an established transgenic mutation model such as the Big Blue® mouse,[35] in which mutation assays have been found statistically reliable and recommended for cancer risk assessment.[36] Alternatively, techniques can be employed such as recently described by researchers at the US Food and Drug Administration, Center for Devices and Radiological Health.[37] The progenitor or stem cells of the colon, for which UV phototoxicity is of greatest concern, are located at the base of the colonic crypts about 500 μm below the mucosal surface.[30] These cells are relatively well protected at this depth as the 1/e penetration depth of 340 nm light in normal colon has been measured at just 240 microns.[6] Mutagenicity concerns are further lessened by the rapid, natural shedding and replacement of epithelial cells in the colon.

The ratio image R27 = (F340/F440) has some similarity to a recently published ratio image composed as the division of a 365-nm-excited AF image by a 405-nm-excited AF image and used to discriminate adenomatous polyp regions from normal colon in sectioned tissue specimens.[26] We expect the ratio image R27 to produce better contrast than a 365/405 AF image when imaging *in situ* polyps because it incorporates contrast from both mucosal NADH (F340) and submucosal collagen (F440). Unlike R27, the 365/405 AF image is reported to have only limited influence from the submucosa which the authors partially attribute to hemoglobin absorption.[26]

In this imaging study of surgical specimens we have obtained results indicating that the capability to detect colon neoplasms could be expanded by including both 340 and 440 nm excitation for AF imaging as well as the reflectance bands 480 and 555 nm. These wavelengths incorporate contrast primarily from NADH, submucosal collagen, and hemoglobin. We found a combination of visual scoring and assessment via an optimized numerical contrast metric to be an appropriate approach in identifying formulaic ratio images with good lesion contrast and desirable histograms for viewing. Our data, although limited by sample size, demonstrate a potential to improve on commercially available AF endoscopes using previously unpublished formulaic ratio images. Expanding our sample pool with more low contrast lesions will help in the development of optimized visualization of difficult to identify lesions. Verification work must be performed *in vivo* following construction of a novel endoscope.

Acknowledgments

We would like to thank Dr. Judith Pugh for useful discussions of observed tissue histology, Dr. Ronguang Liang for his input in device development, and Brenda Baggett for assistance with the image analysis. Financial support for this research was provided by the ARCS Foundation, the Marshall Foundation, the Department of Medicine at the University of Arizona, and the Technology and Research Initiative Fund. Hardware for this instrument was supported in part by NIH, R01CA098341.

References

1. J. C. van Rijn et al., "Polyp miss rate determined by tandem colonoscopy: a systematic review," *Am. J. Gastroenterol.* **101**(2), 343–350 (2006).
2. B. J. Rembacken et al., "Flat and depressed colonic neoplasms: a prospective study of 1000 colonoscopies in the UK," *Lancet* **355**(9211), 1211–1214 (2000).
3. D. K. Rex, "Maximizing detection of adenomas and cancers during colonoscopy," *Am. J. Gastroenterol.* **101**(12), 2866–2877 (2006).
4. R. M. Soetikno et al., "Prevalence of nonpolypoid (flat and depressed) colorectal neoplasms in asymptomatic and symptomatic adults," *JAMA* **299**(9), 1027–1035 (2008).
5. M. Kara et al., "Autofluorescence-based detection of early neoplasia in patients with Barrett's esophagus," *Dig. Dis.* **22**(2), 134–141 (2004).
6. K. T. Schomacker et al., "Ultraviolet laser-induced fluorescence of colonic tissue: basic biology and diagnostic potential," *Lasers Surg. Med.* **12**(1), 63–78 (1992).
7. R. M. Cothren et al., "Gastrointestinal tissue diagnosis by laser-induced fluorescence spectroscopy at endoscopy," *Gastrointest. Endosc.* **36**(2), 105–111 (1990).
8. R. S. DaCosta et al., "Confocal fluorescence microscopy, microspectrofluorimetry, and modeling studies of laser-induced fluorescence endoscopy (LIFE) of human colon tissue," L. J. Steven, Ed., *Proc. SPIE* **2975**, 98–107 (1997).
9. Y. Sun et al., "Fluorescence lifetime imaging microscopy for brain tumor image-guided surgery," *J. Biomed. Opt.* **15**(5), 056022 (2010).
10. K. Konig, "Clinical multiphoton tomography," *J. Biophotonics* **1**(1), 13–23 (2008).
11. J. Wu, M. S. Feld, and R. P. Rava, "Analytical model for extracting intrinsic fluorescence in turbid media," *Appl. Opt.* **32**(19), 3585–3595 (1993).
12. H. Zeng et al., "Spectroscopic and microscopic characteristics of human skin autofluorescence emission," *Photochem. Photobiol.* **61**(6), 639–645 (1995).
13. J. Y. Qu, Z. Huang, and J. Hua, "Excitation-and-collection geometry insensitive fluorescence imaging of tissue-simulating turbid media," *Appl. Opt.* **39**(19), 3344–3356 (2000).
14. J. Y. Qu and J. Hua, "Calibrated fluorescence imaging of tissue in vivo," *Appl. Phys. Lett.* **78**(25), 4040–4042 (2001).
15. H. Zeng et al., "Real-time endoscopic fluorescence imaging for early cancer detection in the gastrointestinal tract," *Bioimaging* **6**(4), 151–165 (1998).
16. J. Haringsma et al., "Autofluorescence endoscopy: feasibility of detection of GI neoplasms unapparent to white light endoscopy with an evolving technology," *Gastrointest. Endosc.* **53**(6), 642–650 (2001).
17. N. Uedo et al., "Novel autofluorescence videoendoscopy imaging system for diagnosis of cancers in the digestive tract," *Digest. Endosc.* **18**(Suppl. 1), S131–S136 (2006).
18. T. Matsuda et al., "Does autofluorescence imaging videoendoscopy system improve the colonoscopic polyp detection rate?—a pilot study," *Am. J. Gastroenterol.* **103**(8), 1926–1932 (2008).
19. Y. Takeuchi et al., "Autofluorescence imaging with a transparent hood for detection of colorectal neoplasms: a prospective, randomized trial," *Gastrointest. Endosc.* **72**(5), 1006–1013 (2010).
20. D. Ramsoekh et al., "A back-to-back comparison of white light video endoscopy with autofluorescence endoscopy for adenoma detection in high-risk subjects," *Gut* **59**(6), 785–793 (2010).
21. G. Rotondano et al., "Trimodal endoscopic imaging for the detection and differentiation of colorectal adenomas: a prospective single-centre clinical evaluation," *Int. J. Colorectal Dis.* **27**(3), 331–336 (2012).
22. T. Kuiper et al., "Endoscopic trimodal imaging detects colonic neoplasia as well as standard video endoscopy," *Gastroenterology* **140**(7), 1887–1894 (2011).
23. F. J. van den Broek et al., "Clinical evaluation of endoscopic trimodal imaging for the detection and differentiation of colonic polyps," *Clin. Gastroenterol. Hepatol.* **7**(3), 288–295 (2009).
24. S. G. Demos et al., "Near-infrared autofluorescence imaging for detection of cancer," *J. Biomed. Opt.* **9**(3), 587–592 (2004).
25. B. Lin et al., "Characterizing the origin of autofluorescence in human esophageal epithelium under ultraviolet excitation," *Opt. Express* **18**(20), 21074–21082 (2010).
26. K. Imaizumi et al., "Dual-wavelength excitation of mucosal autofluorescence for precise detection of diminutive colonic adenomas," *Gastrointest. Endosc.* **75**(1), 110–117 (2012).
27. D. Li, W. Zheng, and J. Y. Qu, "Two-photon autofluorescence microscopy of multicolor excitation," *Opt. Lett.* **34**(2), 202–204 (2009).
28. N. D. Kirkpatrick, M. A. Brewer, and U. Utzinger, "Endogenous optical biomarkers of ovarian cancer evaluated with multiphoton microscopy," *Cancer Epidemiol. Biomarkers Prev.* **16**(10), 2048–2057 (2007).
29. M. C. Skala et al., "In vivo multiphoton microscopy of NADH and FAD redox states, fluorescence lifetimes, and cellular morphology in precancerous epithelia," *Proc. Natl. Acad. Sci. U. S. A.* **104**(49), 19494–19499 (2007).
30. B. Banerjee et al., "Tryptophan autofluorescence imaging of neoplasms of the human colon," *J. Biomed. Opt.* **17**(1), 016003 (2012).
31. N. D. Kirkpatrick et al., "Endogenous fluorescence spectroscopy of cell suspensions for chemopreventive drug monitoring," *Photochem. Photobiol.* **81**(1) 125–134, (2005).
32. H. Aihara et al., "Numerical analysis of the autofluorescence intensity of neoplastic and non-neoplastic colorectal lesions by using a novel videoendoscopy system," *Gastrointest. Endosc*, **69**(3 Pt. 2) 726–733 (2009).
33. R. Drezek et al., "Understanding the contributions of NADH and collagen to cervical tissue fluorescence spectra: modeling, measurements, and implications," *J. Biomed. Opt.* **6**(4) 385–396 (2001).
34. H. Aihara, H. Tajiri, and T. Suzuki, "Application of autofluorescence endoscopy for colorectal cancer screening: rationale and an update," *Gastroenterol Res. Pract.* **2012** 971383 (2012).
35. S. W. Kohler et al., "Spectra of spontaneous and mutagen-induced mutations in the lacI gene in transgenic mice," *Proc. Natl. Acad. Sci. U. S. A.* **88**(18), 7958–7962 (1991).
36. J. A. Heddle et al., "In vivo transgenic mutation assays." *Environ. Mol. Mutagen.* **35**(3), 253–259, (2000).
37. A. Agrawal and D. E. Godar, "Simultaneous detection and semiquantification of DNA damage in normal and apoptotic cells: triple-immunofluorescent labeling using DAPI, antibodies, and TUNEL," *Appl. Immunohistochem. Mol. Morphol.* **20**(4) 402–409, (2012).